IEEE Access
Multidisciplinary | Rapid Review | Open Access Journal

Received 17 September 2025, accepted 13 October 2025, date of publication 16 October 2025, date of current version 24 October 2025.

Digital Object Identifier 10.1109/ACCESS.2025.3622308

RESEARCH ARTICLE

An Artificial Neural Network-Based Approach for Instantaneous Estimation of the Sea Surface Elevation in a Wave Farm

H. MENDONÇA, (Member, IEEE), S. MARTINEZ, (Senior Member, IEEE), AND R. M. DE CASTRO

Escuela Técnica Superior de Ingenieros Industriales, Universidad Politécnica de Madrid, 28006 Madrid, Spain

Corresponding author: H. Mendonça (hugo.rocha@upm.es)

This work was supported in part by Spanish Ministry of Economy and Competitivity under Grant ENE2012-36981, and in part by the OPS Master Plan for Spanish Ports is co-financed by the Connecting Europe Facility (CEF) for the Building of European Union's TEN-T under Project 2015-EU-TM-0417.

ABSTRACT Many control strategies to maximise the captured power by wave energy converters depend on the knowledge of the incoming wave in a short term future. However, the wave prediction may be unpractical in a wave farm, since many measurement systems would be required. As a part of a prediction system, this paper presents an estimator of the instantaneous sea surface elevation in an open-field sea area for potential wave farm deployment based on a single measurement point. The approach is based on a time delay artificial neural network and the paper explores the performance of the estimation for a given field and the sensitivity to different sea characteristics. The proposed realisation of the artificial neural network is found to be accurate and robust, resulting in a useful tool for a wave prediction system in a farm for control purposes.

INDEX TERMS Artificial neural network, time delay neural network, wave energy converter, wave estimation, wave farm.

I. INTRODUCTION

One of the main challenges in the field of wave energy is to reduce the levelized cost of energy, and several aspects have to be considered to reach this goal. One of them is to improve the efficiency of wave energy conversion into electrical energy without compromising cost. As a rule, the wave energy converter (WEC) should operate in an ideal operating point [1]. This is an essential factor to make wave power plants able to recover the investments through fuel cost savings [2]. One way to achieve this improvement is to maximise the energy generated by a WEC. In this sense, many control strategies have been proposed – some of them are general and others specific to particular devices. The main strategies are gathered and presented with extended comparisons among them in [3] and [4]. It can be seen that, for example, to implement discrete controls, latching and declutch, the estimation of the excitation wave force may be required, and, for this, the prediction of the sea surface could be used.

For feasible exploitation of the wave energy, large wave farms will be required, like wind energy. So, in the case of point absorbers, a wave farm would be composed of tens or hundreds of WECs. This results in the so-called park effect [5], where the total power of the farm is, in general, less than the total power produced by one WEC multiplied by the number of WECs in the farm. Hence, it is even more critical to ensure the WEC operation is in, or very close to, the ideal operating point. In this sense, the improvement of the efficiency of every single converter is closely related to the wave prediction in a short time horizon. In [6], another approach is presented, where the wave farm controller must take into account two aspects: to maximise the effects of constructive interferences of the waves caused by the WECs and to minimise the effects of their destructive interferences. In addition, [7] points out the importance of up-wave surface

The associate editor coordinating the review of this manuscript and approving it for publication was Domenico Rosaci.

elevation knowledge to provide a smooth hydrodynamic control. Furthermore, this information can be also useful, from the wave farm controller point of view, to both mitigate the impacts on the electrical grid and accomplish some grid requirements [8].

In summary, the availability of wave prediction can contribute to a better WEC control in a farm. The wave prediction can be mainly carried out by two methods: **(i)** the first one is based on single-point measurements, where the WEC is responsible for recording the observed wave and, also, to provide a wave prediction for its own location; and **(ii)** the second one is based on a spatial reconstruction of the wavefield with available up-wave information from one or more nearby sensors.

According to [9], the approach **(i)** has considerable advantages with respect to **(ii)**, such as simpler forecast model and less amount of instrumentation required. It presents different models for short-term wave prediction, such as cyclical models, extended Kalman filter, autoregressive (AR) model and neural networks. All of them provide a wave prediction within a limited horizon time by using past wave elevation data at the WEC location. The work in [9] concludes that a simple AR model is enough to provide a very accurate prediction. This approach applies a low-pass filter to the wave data time series by using a zero-phase filter, i.e., no phase shift is added and, therefore, the original signal is preserved. However, this filtering process might not fit for real-time application because of inherent added delays to the original signal and it has to be further studied.

The approach **(ii)** lies in the deterministic sea wave prediction (DSWP). This technique is capable of predicting the propagated sea surface by measuring the sea surface elevation at some distance [10], usually within a time horizon of tens of seconds. This approach uses a linear filter to provide the dispersive phase shift to the DSWP model. The filter methodology reduces the computational effort compared to other methods as the one developed by [11]. On the other hand, [12] uses digital filters to translate the pressure and wave phase measured at the up-wave sensor to determine the resulting surface elevation and phase at the WEC. In [13], a space-time diagram is presented that defines the region where sea surface measurements influence future wave behavior, based on the dispersion relation for linear waves. In addition, it provides guidelines to assess a DSWP model in terms of prediction time, prediction space and accuracy.

Radar has been used to obtain sea surface data for DWSP models in [11], [14] and [15] with X-band radar, and for model predictive control in [16] with Doppler radar. This technology scans a sea area and provides high resolution images of the sea surface in both spatial and temporal variations. In addition to radars, that operate with electromagnetic microwaves, lidar technology can also be found for this application. A sea surface image is formed from laser pulses [17], [18].

Another way to obtain these data is from up-wave sensors. For example, [19], [20] propose spatio-temporal predictors of the wave field based on Gaussian sea waves. However, both methodologies require the availability of several measurement spots. In a similar approach, [21] uses a hydrostatic wave pressure sensor (a near-shore air-chamber at about 60 meters of distance) to determine the sea surface elevation at this point.

Nevertheless, what if both the sea surface elevation measurements at the WEC and at the up-wave sensor are available? This is the case of Pico OWC shown by [21]. They use artificial neural networks (ANN) to forecast the chamber hydrodynamics from the hydrodynamic data measured by the hydrostatic wave pressure sensor. As a result, hydrodynamic forecasts present a satisfactory accuracy.

On the other hand, [22] focused on the sea surface elevation only. They brought together the AR model for short-time prediction [9] and the model used to predict the sea surface elevation at the OWC from the up-wave measurements. Finally, an autoregressive with exogenous (ARX) input model is built. It is important to highlight that the contribution of extra data to the AR model, in this case, the exogenous input, might make the prediction model more robust and then improve forecast accuracy.

A measurement system for every single WEC would have a significant impact on the cost of the farm. Facing this scenario, this work proposes the instantaneous up-wave forecast within a wave farm from one measurement spot. As the relation between the measurement spot and any spot at the wave farm could only be described by a complex wave-structure interaction model heavily based on physics, the ANN provides an alternative for building the nonlinear dynamic model from input/output wave data and then to estimate the sea surface elevation within a wave farm. Using this tool as part of a prediction system would allow the use of just one measurement and prediction system for a whole farm. This approach is justifiable in regions where the wave climate presents small changes and a well-defined swell component. Thereby, a wave measurement campaign should be carried out to provide different possible data scenarios and, thus, to avoid the development of new models. It is important to note that the objective of this study is not to propose or evaluate a specific wave farm layout, but rather to assess the feasibility of the proposed methodology for mapping wave elevation over an open-sea area using only a single measurement spot.

ANNs have been successfully used for system identification in many fields. Focusing on their applications in the marine environment, [23], [24] provide a comprehensive literature review on ANN architectures and their various applications. The ANN architecture is usually represented by the scheme [(a)-(b)-(c)], the feedforward neural networks, known as multilayer network (MLN), where (a) is the input layer, (b) represents the hidden layers, and (c) the output layer. For example, the MLN has been used by [25] to estimate

statistical parameters of the sea in a very particular area – within a harbour – characterized by fully nonlinear waves and by [26] to estimate the breaking wave height.

This architecture is a universal function approximator [27] because it can be easily adapted to process time series by introducing a memory structure to the model. This last structure was first introduced by [28] for phoneme recognition where each weight is associated with a delay. Thus, an interesting ANN architecture is designed taking into account the temporal aspects of the input: the time delay neural network (TDNN). In addition to this, there are ANN architectures that are more robust for nonlinear system identification, such as recurrent neural networks (RNN), which are capable of selectively remembering or forgetting information. Within this latter architecture, one can find Long Short-Term Memory (LSTM), which includes an internal memory and is able to learn dependencies over time, although it is more complex. LSTM networks have been used by both [29], [30] to estimate the significant wave height. Another RNN, the Nonlinear AutoRegressive models with eXogenous inputs (NARX) [31], has shown to be well suited for this task in many different fields, including time series. NARX models have been applied for nonlinear identification in different fields [32], [33], [34], [35], [36]. The input of the NARX model, besides taking into account past values of the input signal, includes past values of the output. However, the central idea of this study is to estimate instantaneously the sea surface elevation within a wave farm with the minimum possible measurement points: only one. Thus, this condition rules out any RNN, despite having more accurate results.

This paper compiles the main results of the first author's Ph.D. dissertation [37] and it is organised as follows. Section II makes a brief description of irregular wave models used along this work. Section III introduces the foundation of ANNs and their architectures, and Section IV presents the application of TDNNs to wave estimation. Section V explores how the ANN configuration affects the estimation performance. Section VI analyses sensitivity of wave estimation to the wave front angle and the sea state for long-crested seas. Section VII assesses the quality of the estimation with respect to the degree of wave spreading in short-crested seas. Finally, Section VIII summarises the conclusions of this work.

II. IRREGULAR WAVE MODELS

Because of the non-stationary and non-deterministic nature of ocean waves, it is impossible to exactly determine the elevation of the sea surface at a pre-determined point in time. However, the amount of energy can be represented statistically by the wave spectrum. More formally, the variance density spectrum, that is usually related to the wave frequency, f, describes the the statistical properties of the sea surface elevation. These properties define the sea state, which can be represented by two parameters: significant wave height, H_s, and energy period, T_e. Both parameters can be calculated directly from the wave spectrum and they are also known as statistical wave parameters.

One of the most widely used wave spectra is the Bretschneider spectrum [38]. A modified version with two parameters, ITTC spectrum, which can be found in [38], is used in this work and can be described in terms of H_s and T_e as follows:

$$S(f) = \frac{A}{f^5} \exp\left(-B/f^4\right) \tag{1}$$

with:

$$A = \frac{0.0081}{K^4} g^2 \; ; \; B = \frac{0.0081}{K^4} \frac{4g^2}{H_s^2} \; ; \; K = \frac{T_e}{2.137} \sqrt{\frac{g}{H_s}} \tag{2}$$

where g is the gravitational acceleration.

A realisation of the sea surface elevation in a wave farm can be generated by the superposition of a large number of regular waves, each with an amplitude taken from the given spectrum and a random phase angle:

$$\zeta(x, y, t) = \sum_{n=1}^{N} \sqrt{2S(f_n)\Delta f} \times \sin\left[2\pi f_n t - k_n(x \cos \chi_1 - y \sin \chi_1) + \varepsilon_n\right] \tag{3}$$

where f_n is each individual frequency considered and k_n and ε_n are their corresponding wave number and phase angle, Δf is the frequency resolution, x and y the coordinates at the wave farm, and χ_1 the wave front angle.

For example, for the wave realization in the following sections of this paper, the number of frequencies used, N, is defined by the quotient between the spectral bandwidth of the wave and the frequency resolution $\Delta f = 0.1$ Hz. The spectral bandwidth is divided into N evenly spaced frequency ranges within which the corresponding f_n is randomly selected. Similarly, the phase angle, ε_n is randomly selected in a $[0, 2\pi]$ interval.

This model is known as long-crested sea, where regular swell waves travel in the same direction and they have longer periods and lengths than in chaotic seas within the fetch area, where waves are originated (Figure 1). In the dispersion area, waves become more regular, changing to swell waves whose periods range from 5 to 30 seconds and they are usually limited by shorelines. In addition, the most part of the energy of swell waves generated in the fetch area is transported over long distances with little decay [39].

On the other hand, more than one direction of wave propagation might appear in the sea resulting in a short-crested sea. Despite this type of sea is more common in fetch areas, it is possible to find swell waves travelling with different directions whose interactions result in short-crested seas outside the fetch area, with waves characterised by shorter lengths and periods. Therefore, seas with different periods, heights and lengths propagating in different directions appear (Figure 1). The sea state can be modelled from a composition of wave and directional spectra: $S(f, \chi) = S(f)G(\chi)$, where the spreading function G depends on the direction of the wave

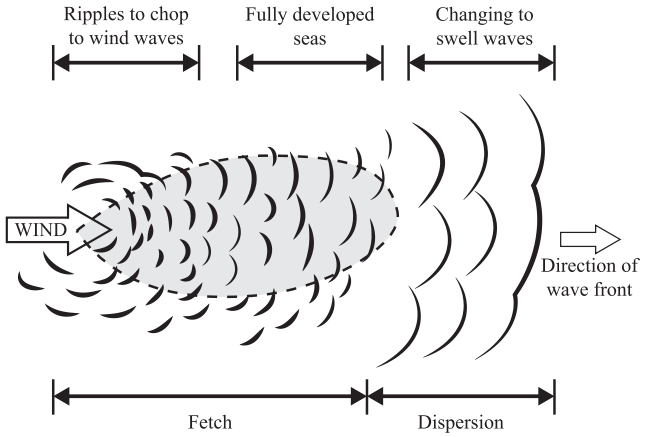

FIGURE 1. Irregular seas in the fetch and dispersion areas (based on [40]).

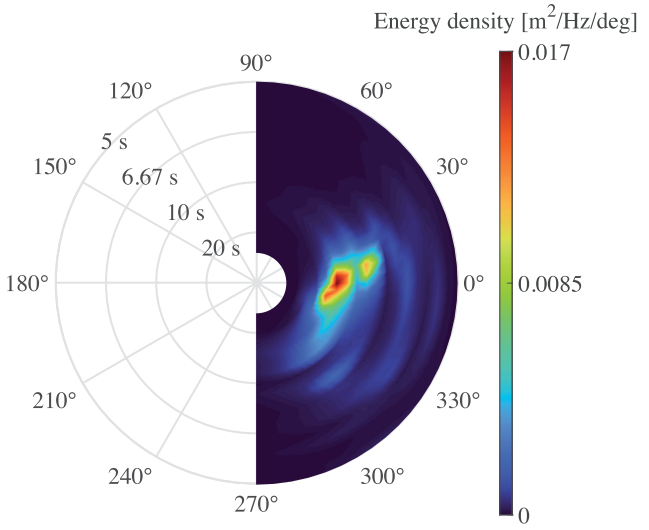

FIGURE 2. Directional wave spectrum of CDIP buoy 43 (data from CDIP, Scripps Institution of Oceanography).

propagation χ. Reference [38] defines as the most common spreading function:

$$G(\chi) = \frac{2^{2s-1}}{\pi} \frac{\Gamma^2(s+1)}{\Gamma(2s+1)} \cos^{2s}(\chi - \chi_1) \tag{4}$$

where χ_1 is the main direction of wave propagation, s is the width of the directional spread and Γ is the gamma function. The realisation of the sea is similar to Equation (3), but now it takes into account the angles of wave propagation:

$$\zeta(x, y, t) = \sum_{n=1}^{N} \sum_{m=1}^{M} \sqrt{2S(f_n, \chi_m)\Delta f \Delta \chi} \times \sin\left[2\pi f_n t - k_n(x \cos \chi_m - y \sin \chi_m) + \varepsilon_n\right] \tag{5}$$

where M is the number of directions of wave propagation, and $\Delta\chi$ is the propagation angle resolution.

For example, for the short-crested sea realization in the following sections of this paper, the number of directions of wave propagation used, M, is defined by the quotient between the considered wave propagation angle bandwidth and the propagation angle resolution $\Delta\chi = 5°$. In addition, the width of the directional spread used is $s = 2$.

To illustrate a real wave spectrum, let us consider the directional spectrum shown in Figure 2, corresponding to observations from buoy 43 of the Coastal Data Information Program (CDIP) located in the west coast of the United States (GPS coordinates: 33.2198°, −117.4394°). The directional spectrum was calculated from wave measurements on 12-11-2016 from 11:02 to 11:32 and it is free available in [41]. It is possible to identify the direction to which waves are traveling and that the highest energy is spread in a narrow band around 240°. Thus, the most part of the energy is carried by a predominant wave in this direction of propagation. Therefore, for this scenario, it is reasonable to think that the prediction should be focused on the main direction.

III. ARTIFICIAL NEURAL NETWORK

The most simple structure of an ANN is the perceptron, presented by [42], in which there is just a single unit (artificial neuron) able to classify objects according to their classes. The artificial neuron (or cell-body) is composed of a sum block and an activation function and its response. Therefore, it is a function of the weighted sum of all inputs and a bias. This activation function can be defined in different forms, such as linear, step, ramp, sigmoid, hyperbolic tangent and gaussian, depending on its application. A combination of two or more neurons results in a network with one or more layers. This is the most common neural architecture known as multi-layer perceptron (MLP). A MLP is a feed-forward network composed of perceptrons arranged in layers. These layers are: input layer, one or more hidden layers, and output layer. Therefore, a MLP has 3 layers at least.

If the perceptron is adapted to receive a temporal information, its independent inputs are changed into time-lagged inputs. This model is a typical dynamic neural architecture, whose response to a tapped delay line input is given by:

$$y[k] = f\left(\sum_{i=0}^{p} w_{ji} x[k-i] + b_j\right) \tag{6}$$

where $y[k]$ is the current data, p is the tapped delay length, w_{ji} is the weight from the i-th input neuron to the j-th neuron ($j = 1$ for the perceptron), b the bias, and $f(\cdot)$ is the activation function. In addition, if the activation function of this type of ANN is linear, one can conclude that this model is a neural equivalent to the ARX model presented by [22] with no poles. Several dynamic neural models can be found in [43].

A. TIME DELAY NEURAL NETWORK (TDNN)

The TDNN architecture is based on a typical MLP feedforward network, but with a tapped delay line. In addition, most of TDNN systems also present feedback inputs. TDNN has been mostly used in speech recognition applications [44], [45].

Nevertheless, the TDNN application has been extended to other fields as commented before. For example, it could be applied to predict wind speed and solar radiation [46], [47]; rainfall [48]; traffic flow [49], [50], [51]; etc. Also, TDNN could be used to dynamic system identification. Reference [34] shows that, despite the high nonlinearities presented in an uncrewed helicopter system, TDNN can lead to very accurate models. Moreover, other techniques can be used with TDNN to improve its performance as commented by [52] and to reduce order model as shown by [32].

In this sense, this work seeks to identify the nonlinear model of the wave-field propagation. The model must be able to estimate the sea surface elevation at any point within an area from a measurement of the sea surface elevation at a single spot. Therefore, each estimation spot has its own estimation system with a single signal input from the measurement spot.

The TDNN structure for the estimation model is presented in Figure 3. This is a typical MLP feedforward network, but with a tapped delay line. Note that z^{-1} is the unit delay and the neuron structure is represented by a filled grey circle for simplification. The estimated value $\hat{y}[k]$ depends on the previous values of the input $x[k]$. Therefore, the system can be described by:

$$\hat{y}[k] = f\left(x[k], x[k-1], x[k-2], \ldots, x[k-p]\right) \tag{7}$$

This architecture is modelled as a composition of weighted sum as follows:

$$\hat{y}[k] = f\left[\sum_{j=1}^{h} w_j^{(2)} \cdot g\left(\sum_{i=0}^{p} w_{ji}^{(1)} x[k-i]\right)\right] \tag{8}$$

where h is the number of neurons in the hidden layer. In this network, the sigmoid and the linear functions are used in the hidden and output layers, respectively.

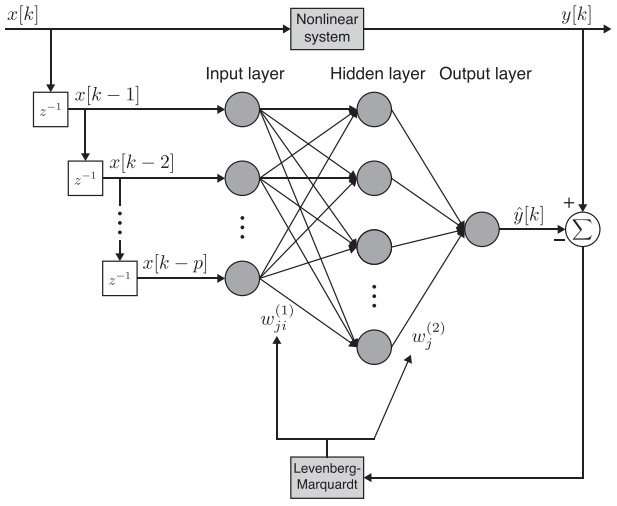

FIGURE 3. Feedforward neural network structure with a tapped delay line.

The learning algorithm used is the Levenberg-Marquardt [53], that is a usual optimisation technique to solve nonlinear least squares problems, which, in this case, results in the adjustment of the network weights. The learning method must minimise a cost function, for example, the mean square error (MSE):

$$\text{MSE} = \frac{1}{N}\sum_{k=1}^{N}\left(y[k] - \hat{y}[k]\right)^2 \tag{9}$$

In addition, it can be said that this learning algorithm has been shown to be fast, accurate and efficient, even applied to a simple structure of the ANN model as verified by [54], where a simple configuration was used to predict a chaotic time series.

IV. TDNN APPLICATION TO WAVE ESTIMATION

To assess the quality of the wave estimation in different spots within a wave farm from a measurement spot, wave data series for long-crested seas have been mathematically generated according to Equation (3), with a wave front angle $\chi_1 = 0°$, for a duration of 2000 seconds, sampled at 2 Hz, with the following wave statistical parameters: $H_s = 2$ m and $T_e = 8$ s. The spectral bandwidth used is 20 Hz, giving place to $N = 200$ in Equation (3). In addition, the wave data series have been generated with different wave front angles. Figure 4a shows the wave farm topology analysed in this work, whose area is 8000 m^2, and Figure 4b illustrates one wave data series at the measurement spot. The estimation spots are numbered from 1 to 100 and the measurement spot is marked with a cross. The spots stand 10 m apart from each other in both axis, x and y.

The TDNN is then configured and trained in MATLAB/Simulink to estimate the sea surface elevation within the wave farm. The first 1000 s of the wave data are used to train the TDNN and the remainder is used to test it and to evaluate its performance. As mentioned before, the Levenberg-Marquardt algorithm is used to train the TDNN and the training results are evaluated by the MSE. The training-validation process is stopped when a new iteration leads to an increase of the MSE. Note that the TDNN-based estimator so trained is the one used in all the following sections.

The trained TDNN is tested with the other 1000 s of the wave data. The estimation at each spot can be assessed by comparing the estimated with the pseudo-measured data. The assessment is carried out according to the R^2 value which is calculated as follows:

$$R^2 = 1 - \frac{SS_{res}}{SS_t} \tag{10}$$

where $SS_t = \sum_k (y_k - \bar{y})^2$ is the total sum of squares, $SS_{res} = \sum_k (\hat{y}_k - y_k)^2$ is the residual sum of squares, y is the measured data, $\bar{y}$ the mean of the measured data and $\hat{y}$ is the estimated data. The higher R^2 value (the closer to 1), the better estimation [55]. So the R^2 value is calculated for each estimation spot and, to evaluate the overall estimation in the wave farm, the average of all R^2 values is also calculated.

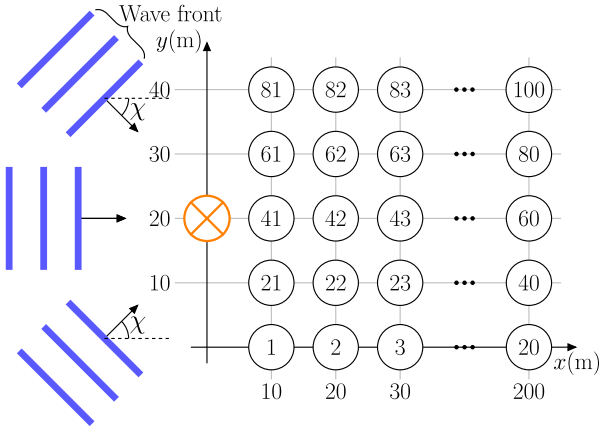

(a) Incident wave fronts in a wave farm with one hundred estimation spots from a measurement spot (marked with a cross).

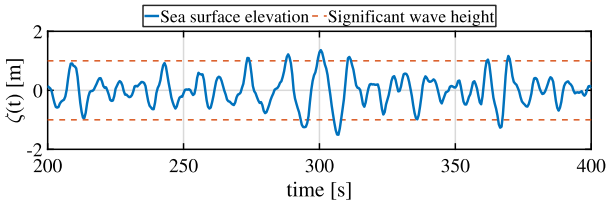

(b) Sample of wave data series at the measurement spot.

FIGURE 4. Wave farm topology.

V. EFFECTS OF THE ANN CONFIGURATION

In any ANN architecture, its configuration plays a key role in the performance. The main drawback of the ANN is its closed box model where there is no control on the calculation. So, usually, the best parameters are obtained after several trials by selecting the network with the best performance. In this sense, this section studies the effect of the number of neurons and tap delays on the estimation performance. Assuming that the wave front is perpendicular to axis-x, i.e., it is at $\chi_1 = 0°$, all the spots along axis-y have the same sea surface elevation, since a long-crested wave is considered. Therefore, in this section, the TDNN is trained with the spot array from 41 to 60 and the measurement spot at the position (0, 20).

The ANN has been trained and tested to between 1 and 50 hidden neurons, and to between 10 and 100 tap delays. Sweeping all configurations, the average R^2 value is calculated from each spot estimation and it is shown in Figure 5. It is verified that the longer the tap delay, the better the estimation. For short tap delays, the results indicate a nonlinear relationship for the model. Besides, it is possible to see that the improvement of the R^2 value for tap delays longer than 80 is not significant, what leads to conclude that a much longer tap delay line results in a higher computational effort without a considerable estimation improvement. In addition, for each tap delay curve in Figure 5, it is seen that, from a certain number of hidden neurons, the estimation performance is not affected.

The estimation performance is not only affected by the TDNN configuration, but also by the distance of the

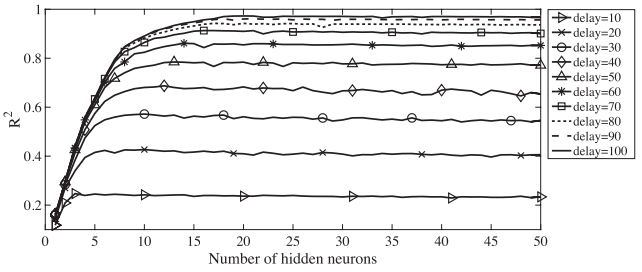

FIGURE 5. Average R^2 for the number of hidden neurons and tap delays.

estimation spot from the measurement spot. According to Figure 5, the best TDNN architecture is [100-20-20], i.e., one hundred neurons in the input layer (tapped delay length); one hidden layer with twenty neurons, since, for the best fitted model (100-tap delay), this number of hidden neurons is enough; and one output layer with twenty neurons (the spot array from 41 to 60). For this TDNN configuration, Figure 6 shows the R^2 values with respect to the number of tap delays and the distance from the measurement spot. It is clear that the closer the estimation spot to the measurement spot, the better the estimation. However, for taped delays longer than 80, it is possible to get a very good estimation at the farthest spots. Thus, this TDNN architecture ([100-20-20]) shows to be adequate to estimate the wave surface elevation in the wave farm from a measurement spot.

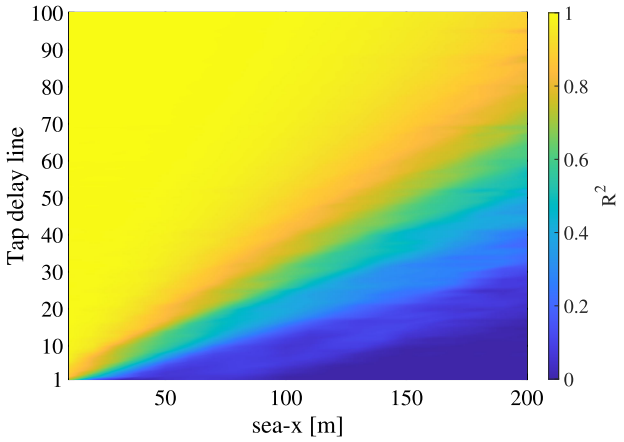

FIGURE 6. R^2 value with respect to the number of tap delays and the position in the wave farm.

VI. SENSITIVITY ANALYSIS OF THE WAVE ESTIMATION

In this section, the sensitivities of the wave estimation with respect to the wave front angle and the sea state are analysed. To assess the estimation for a given spot in the wave farm, the TDNN architecture with twenty hidden neurons is used. However, unlike the previous model, the output layer has one hundred neurons (the total number of estimation spots). In other words, the new TDNN is [100-20-100]. The first analysis is carried out with three irregular (long-crested) wave data series whose wave front angles χ_1 are at 0°,

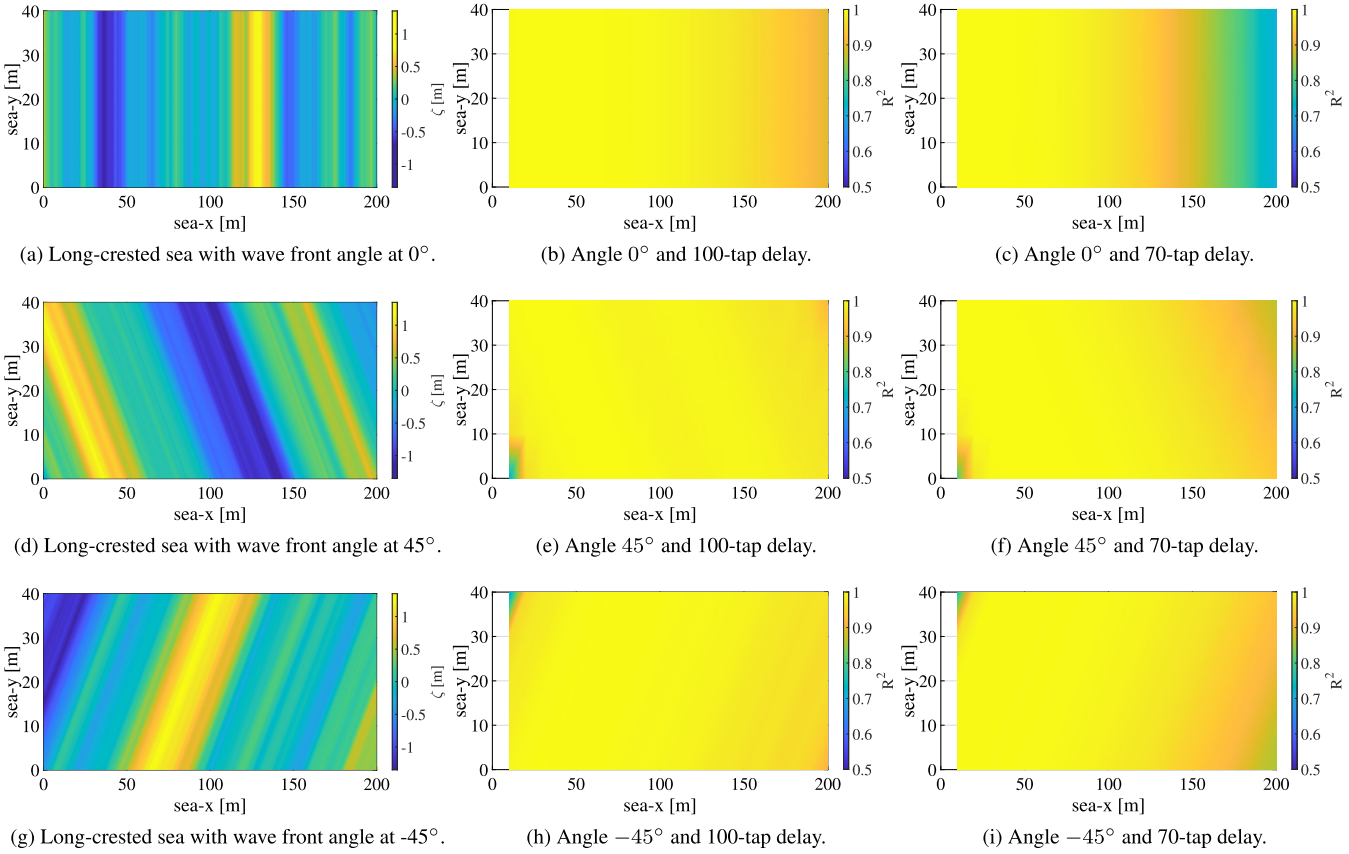

(a) Long-crested sea with wave front angle at 0°. (b) Angle 0° and 100-tap delay. (c) Angle 0° and 70-tap delay.

(d) Long-crested sea with wave front angle at 45°. (e) Angle 45° and 100-tap delay. (f) Angle 45° and 70-tap delay.

(g) Long-crested sea with wave front angle at -45°. (h) Angle −45° and 100-tap delay. (i) Angle −45° and 70-tap delay.

FIGURE 7. R^2 value for the wave estimation in the wave farm with 100- and 70-tap delays, and wave front angle χ_1 at 0°, 45° and −45°.

45° and −45° with respect to the axis-x, as shown in Figure 4. In addition, a comparison between the TDNN with 100- and 70-tap delay line is presented. Note that, for the 70-tap delay, some estimation spots present R^2 values bellow 0.8, as it can be seen in Figure 6. The TDNN has been trained for each wave front angle and for both tapped delays.

As a result, Figure 7 shows the R^2 value for each scenario. It can be seen that, for 100-tap delay, the wave estimation has a very good quality for all of the three wave front angles. Also, it can be said that for different angles, the estimation is not as good as for 0°, but it still has a good estimation quality. For example, Figures 7e and 7h show the R^2 values for wave front angles at 45° and −45° being mostly around 0.9, except for the extremes where the incoming wave reaches the estimation spot before the measurement spot. An interesting fact is that those extreme spots present a better quality estimation for the 70-tap delay, but the overall quality of the estimation is better for the 100-tap delay line. Note that, for wave front angles at 45° and −45°, the R^2 values might be symmetrical. However, it is not perfectly symmetrical, as in the case of Figure 7a, because for each training of the TDNN, different solutions are given. Finally, the worst estimation spots are identified by comparing Figures 4a and 7. For a wave front angle at 0°, they are 20, 40, ..., 100 – the orthogonal points farthest from the measurement spot – and for wave front angles at 45° and −45°, they are 1 and 81, respectively – the corners of the first column of positions just beyond the measurement spot where the wave front takes the longest to arrive.

A. WAVE FRONT ANGLE

To evaluate how the wave front angle χ_1 affects the wave estimation, the TDNN is firstly trained for a wave data series in which the wave front angle is 0°. Then, wave data series have been generated with wave front angles between −45° and 45° within the wave farm in Figure 4a. The latter series have been used as the input data to the TDNN-based estimator previously trained with wave front angle 0°. The average R^2 value of the wave estimation in the farm is shown in Figure 8. Note that R^2 value is symmetrical as said before. In addition, it is possible to conclude that the wave estimation within the wave farm presents a high dependency on the main direction of the front wave. Nonetheless, under these conditions, it is possible to say that for wave front angle deviations up to ±10°, the estimation quality is still very good. For example, for wave front angle −10°, the average R^2 value is about 0.9. This can be seen as a robustness test showing the behaviour of the technique when it is not very adequately used. In this case, the TDNN is trained as if there were just one wave direction in the farm (what it is not true),

just to show that even when so poorly trained, the TDNN can give not so bad estimations. Note that a wave farm must be settled in a sea area previously studied with several weather conditions recorded. Based on this, it would be possible to have the ANN model trained for different scenarios of directional spectrum.

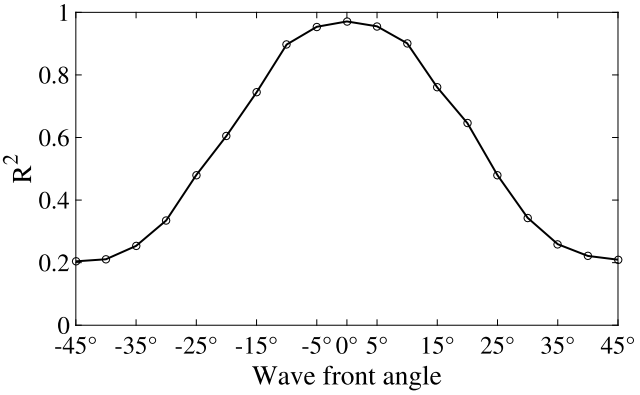

FIGURE 8. Sensitivity of the wave estimation to the incident wave front angle χ_1.

B. SEA STATE

Although the wave statistical parameters tend to remain constant between consecutive 30-minute time windows, they can change, albeit slightly. In other cases, they may undergo major changes over a day, for example, during a storm. So it is important to consider how these changes may affect the wave estimation.

As stated in Section IV, the TDNN is trained for irregular (long-crested) wave data series whose wave statistical parameters are $H_s = 2$ m and $T_e = 8$ s with unidirectional waves at zero-degree incidence. Here, several wave data series with the same wave front angle, but different wave statistical parameters, have been generated. The latter series have been used as the input data to the TDNN-based estimator. After estimating the sea surface elevation within the wave farm, the average R^2 value is calculated for each combination of significant height and energy period. These results are shown in Figure 9a, where it can be seen that most of the average R^2 values are between 0.9 and 1, with a minor portion from 0.8 to 0.9. Thus, one can conclude that the overall estimation is quite satisfactory. On the other hand, if the same TDNN is applied to estimate wave series with different wave statistical parameters and a different wave front angle, the estimation shows a worsening compared to the previous one, as it can be seen in Figure 9b for the case of 10°. None average R^2 value is close to 1, and, for the most part of the farm, the values are between 0.6 and 0.9.

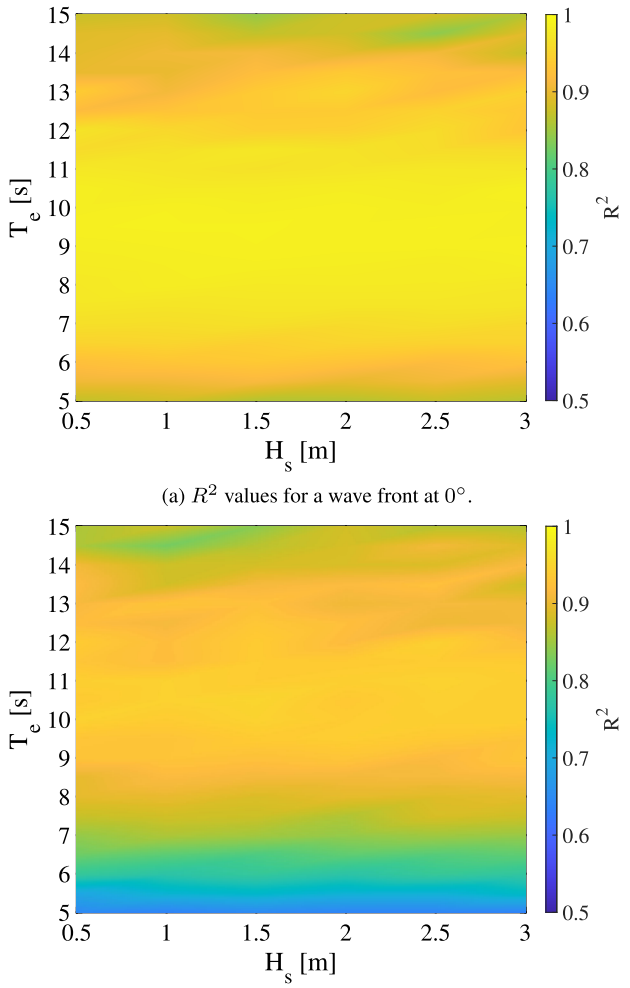

(a) R^2 values for a wave front at 0°.

(b) R^2 values for a wave front at 10°.

FIGURE 9. Sensitivity of the wave estimation to the statistical wave parameters for an ANN trained with a wave front at 0°.

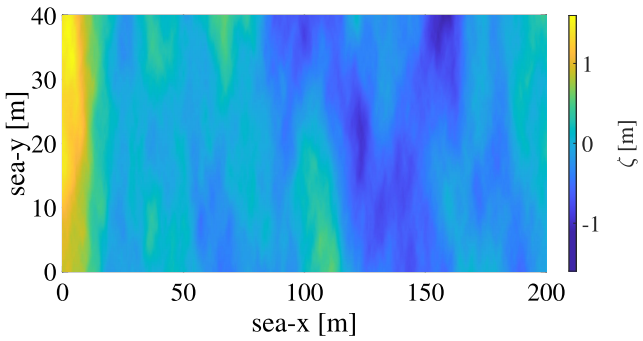

FIGURE 10. Three-dimensional representation of the sea surface elevation at a given time instant.

VII. SHORT-CRESTED SEA ESTIMATION

Despite the fact that in many cases short-crested seas can be ignored because they do not much affect a floating structure motion [56] and the wave farms might be located in a dispersion zone, outside the fetch area (see Figure 1), where there is almost no energy dispersion, in this section, the quality of the wave estimation is assessed with respect to the degree of wave spreading. The wave data series generated for this analysis have the same characteristics as the case of long-crested seas. However, here, the waves have more than one

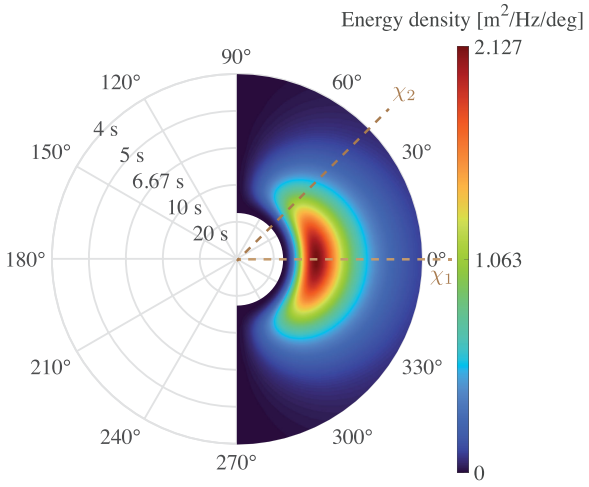

(a) Short-crested sea for two wave directions.

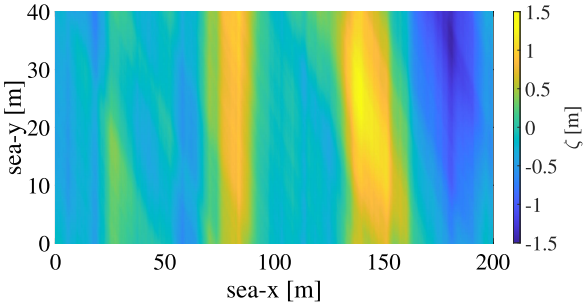

(b) Short-crested sea for two wave directions.

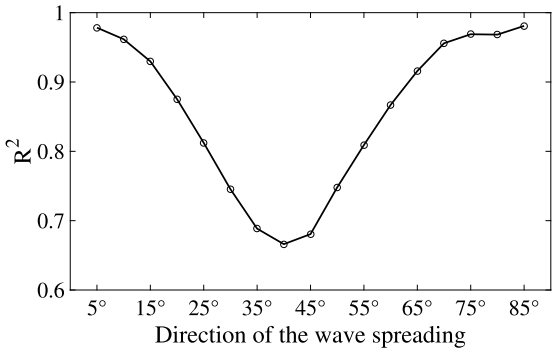

(c) Average R^2 values for one direction of wave spreading.

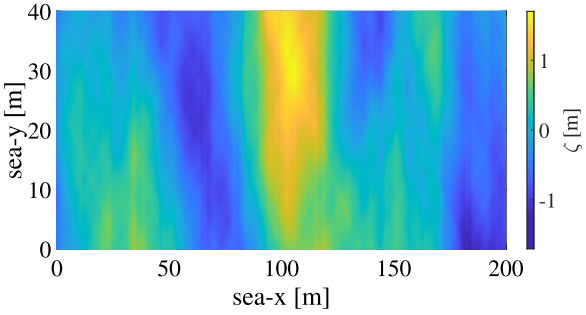

(d) Short-crested sea for three wave directions.

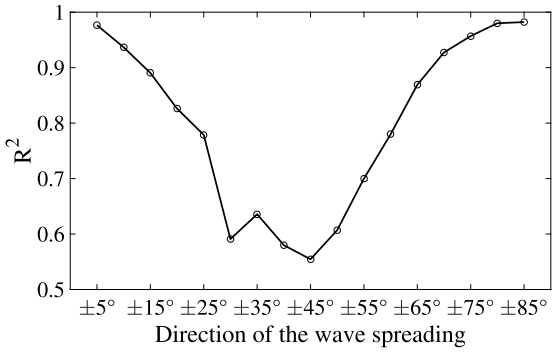

(e) Average R^2 values for two symmetrical directions of wave spreading.

FIGURE 11. **Estimation quality in a wave farm for a sea state with wave spreading.**

propagation direction. Figure 10 shows a three-dimensional representation of the sea surface elevation at a given time instant for the chaotic sea used in the test.

The following analysis are performed with different wave data series, all of them used as input to the same TDNN-based estimator. In a first analysis, to force the estimator to the limits, even to non-realistic scenarios, just to test the robustness of the estimator, only two directions of wave propagation ($M = 2$) are considered: χ_1 and χ_2. Different tests have been carried out with $\chi_1 = 0°$ and χ_2 varied from 5° to 85°. The sensitivity of the estimation to χ is shown in Figure 11c, where it is verified that the best estimation is achieved for wave spreading close to the main wave propagation direction. Note that good estimations beyond about 45° are only due to the formulation used for the spreading function (Equation 4). Similarly, the estimation quality when the energy spreads in two symmetrical directions is shown in Figure 11e. In this case,

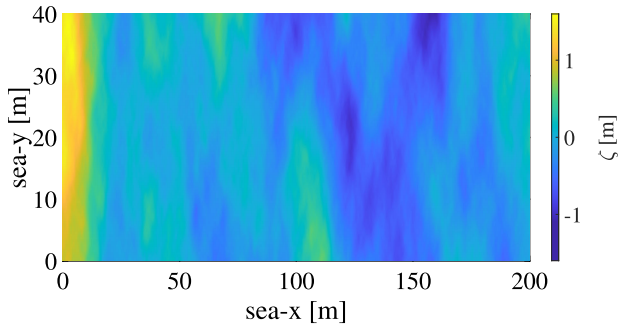

(a)

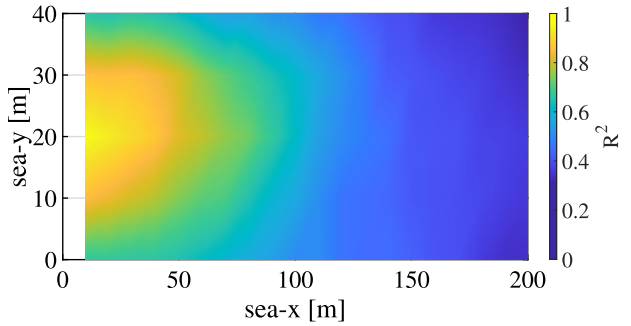

(b) R^2 values in a farm for chaotic sea.

FIGURE 12. Estimation quality in a wave farm for wave field generated by directional ITTC spectrum.

three directions of wave propagation ($M = 3$) are considered. The results are similar to the obtained for the one direction case, but the average R^2 value found is slightly worse. However, for both cases, directions of wave spreading up to 15° present a very good estimation with average R^2 values greater than 0.9, in general.

In addition to these cases, the estimation quality is assessed for a chaotic sea inside a fetch area. In this particular scenario, the energy spreads in many directions. Figure 12 shows the R^2 values over the wave farm for one wave direction ($\chi_1 = 0°$) and dispersion $\chi \in [-90°, 90°]$. It is seen that beyond 100 m in the axis-x the estimation is not satisfactory. As a conclusion, even in chaotic seas the instantaneous wave estimation can be satisfactory depending on how far the estimation spot is from the measurement spot. Obviously, using the same TDNN-based estimator with other wave directions would lead to poorer results. A similar conclusion can be said about the influence of the width of the directional spread. The higher the s values, the more concentrated the energy around the predominant wave direction, leading to an improvement of the estimation quality, since the wave characteristics tend to a long-crested sea. On the other hand, lower values of s would lead to poorer results, since there is more dispersion.

VIII. CONCLUSION

It is often important to know the incoming wave in a short term future within a wave energy field. This knowledge could be used for control strategies to maximise the captured power by a generating unit (only one WEC). It could also be useful for the farm controller to accomplish some grid requirement. As a wave farm can be composed of tens or perhaps hundreds of WECs, it may be very expensive and unpractical to have a measurement system for each one. In this sense, this work has presented a study about the instantaneous wave estimation in an open-field sea area, for potential wave farm deployment, from a single buoy during operation (although wave-field measurements are required prior to the estimator application).

The TDNN was used to model the behaviour of the waves between the measurement buoy and the estimation spots. This ANN architecture seems to be quite satisfactory for this applications, since it is able to accurately estimate the sea surface elevation in many spots within a wave farm from just one measurement point, even if the farm is inside a fetch area. The influence of the distance of the estimation spot from the measurement buoy and the tapped delay length has been assessed. Naturally, the estimation quality is worse as the distance from the measurement buoy increases. However, depending on the tapped delay length, a very good accuracy in the estimation can be achieved. On the downside, a longer tapped delay leads to an increasing in the TDNN training time. In addition, it is fair to say that its accuracy is highly dependent on the wave front direction and somewhat on the wave statistical parameters. But both training time and its dependence should not be such a problem, since wave farm sites, as in the case of wind farms, should be thoroughly studied before its exploitation and, then, the TDNN must be trained for each possible scenario in order to make this method as effective as possible. In addition, it is important to highlight that its implementation for WEC control purposes in a given farm implies performing the ANN training once the devices are actually deployed, to incorporate the effect of hydrodynamic interactions among them.

Finally, although this study is focused on the use of only one measurement spot, the use of more than one would improve the estimation quality and expand the spatial coverage of the predictions. This work gives a technical tool for further studies, for example, about the optimum number and location of measurement spots.

ACKNOWLEDGMENT

The wave data used in Figure 2 were provided by the Coastal Data Information Program (CDIP), Integrative Oceanography Division, operated by the Scripps Institution of Oceanography, under the sponsorship of U.S. Army Corps of Engineers and California Department of Parks and Recreation.

REFERENCES

[1] A. Ilyas, S. A. R. Kashif, M. A. Saqib, and M. M. Asad, "Wave electrical energy systems: Implementation, challenges and environmental issues," *Renew. Sustain. Energy Rev.*, vol. 40, pp. 260–268, Dec. 2014.

[2] I. Glendenning, "Wave power—A real alternative?" *Ocean Manage.*, vol. 4, nos. 2–4, pp. 207–240, Dec. 1978.

[3] J. Hals, J. Falnes, and T. Moan, "A comparison of selected strategies for adaptive control of wave energy converters," *J. Offshore Mech. Arctic Eng.*, vol. 133, no. 3, Aug. 2011, Art. no. 031101.
[4] J. Xie and L. Zuo, "Dynamics and control of ocean wave energy converters," *Int. J. Dyn. Control*, vol. 1, no. 3, pp. 262–276, Sep. 2013.
[5] A. Babarit, "On the park effect in arrays of oscillating wave energy converters," *Renew. Energy*, vol. 58, pp. 68–78, Oct. 2013.
[6] J. Cruz, R. Sykes, P. Siddorn, and R. E. Taylor, "Estimating the loads and energy yield of arrays of wave energy converters under realistic seas," *IET Renew. Power Gener.*, vol. 4, no. 6, pp. 488–497, Nov. 2010.
[7] U. A. Korde, "Up-wave surface elevation for smooth hydrodynamic control of wave energy conversion in irregular waves," in *Proc. OCEANS-San Diego*, Sep. 2013, pp. 1–10.
[8] H. A. Said and J. V. Ringwood, "Grid integration aspects of wave energy—Overview and perspectives," *IET Renew. Power Gener.*, vol. 15, no. 14, pp. 3045–3064, Oct. 2021.
[9] F. Fusco and J. V. Ringwood, "Short-term wave forecasting for real-time control of wave energy converters," *IEEE Trans. Sustain. Energy*, vol. 1, no. 2, pp. 99–106, Jul. 2010.
[10] M. R. Belmont, J. M. K. Horwood, R. W. F. Thurley, and J. Baker, "Filters for linear sea-wave prediction," *Ocean Eng.*, vol. 33, nos. 17–18, pp. 2332–2351, Dec. 2006.
[11] T. Hilmer and E. Thornhill, "Observations of predictive skill for real-time deterministic sea waves from the WaMoS II," in *Proc. OCEANS-MTS/IEEE Washington*, Oct. 2015, pp. 1–7.
[12] J. Tedd and P. Frigaard, "Short term wave forecasting, using digital filters, for improved control of wave energy converters," in *Proc. 17th Int. Offshore Polar Eng. Conf.*, 2007, pp. 388–394.
[13] L. Abusedra and M. R. Belmont, "Prediction diagrams for deterministic sea wave prediction and the introduction of the data extension prediction method," *Int. Shipbuilding Prog.*, vol. 58, no. 1, pp. 59–81, Jan. 2011.
[14] H. Lund, "Large-scale integration of optimal combinations of PV, wind and wave power into the electricity supply," *Renew. Energy*, vol. 31, no. 4, pp. 503–515, Apr. 2006.
[15] A. Simpson, M. Haller, D. Walker, P. Lynett, and D. Honegger, "Wave-by-wave forecasting via assimilation of marine radar data," *J. Atmos. Ocean. Technol.*, vol. 37, no. 7, pp. 1269–1288, Jul. 2020.
[16] D. Cavaglieri, T. R. Bewley, and M. Previsic, "Model predictive control leveraging ensemble Kalman forecasting for optimal power take-off in wave energy conversion systems," in *Proc. Amer. Control Conf. (ACC)*, Jul. 2015, pp. 5224–5230.
[17] M. R. Belmont, J. M. K. Horwood, R. W. F. Thurley, and J. Baker, "Shallow angle wave profiling LiDAR," *J. Atmos. Ocean. Technol.*, vol. 24, no. 6, pp. 1150–1156, Jun. 2007.
[18] F. Nouguier, S. T. Grilli, and C.-A. Guérin, "Nonlinear ocean wave reconstruction algorithms based on simulated spatiotemporal data acquired by a flash LiDAR camera," *IEEE Trans. Geosci. Remote Sens.*, vol. 52, no. 3, pp. 1761–1771, Mar. 2014.
[19] A. Mérigaud and J. V. Ringwood, "Incorporating ocean wave spectrum information in short-term free-surface elevation forecasting," *IEEE J. Ocean. Eng.*, vol. 44, no. 2, pp. 401–414, Apr. 2019.
[20] A. Fisher, J. Thomson, and M. Schwendeman, "Rapid deterministic wave prediction using a sparse array of buoys," *Ocean Eng.*, vol. 228, May 2021, Art. no. 108871.
[21] K. Monk, D. Conley, M. Lopes, and Q. Zou, "Pneumatic power regulation by wave forecasting and real-time relief valve control for an OWC," in *Proc. 11th Eur. Wave Tidal Energy Conf. (EWTEC)*, 2013, pp. 1–11.
[22] F. Paparella, K. Monk, V. Winands, M. F. P. Lopes, D. Conley, and J. V. Ringwood, "Up-wave and autoregressive methods for short-term wave forecasting for an oscillating water column," *IEEE Trans. Sustain. Energy*, vol. 6, no. 1, pp. 171–178, Jan. 2015.
[23] N. P. Juan and V. N. Valdecantos, "Review of the application of artificial neural networks in ocean engineering," *Ocean Eng.*, vol. 259, Sep. 2022, Art. no. 111947.
[24] A. Pourzangbar, M. Jalali, and M. Brocchini, "Machine learning application in modelling marine and coastal phenomena: A critical review," *Frontiers Environ. Eng.*, vol. 2, Sep. 2023, Art. no. 1235557.
[25] Z. Zheng, X. Ma, Y. Ma, and G. Dong, "Wave estimation within a port using a fully nonlinear Boussinesq wave model and artificial neural networks," *Ocean Eng.*, vol. 216, Nov. 2020, Art. no. 108073.
[26] N. T. Duong, K. Q. Tran, L. X. Luu, and L. H. Tran, "Prediction of breaking wave height by using artificial neural network-based approach," *Ocean Model.*, vol. 182, Apr. 2023, Art. no. 102177.
[27] K. Hornik, M. Stinchcombe, and H. White, "Multilayer feedforward networks are universal approximators," *Neural Netw.*, vol. 2, no. 5, pp. 359–366, Jan. 1989.
[28] A. Waibel, T. Hanazawa, G. Hinton, K. Shikano, and K. J. Lang, "Phoneme recognition using time-delay neural networks," *IEEE Trans. Acoust., Speech, Signal Process.*, vol. 37, no. 3, pp. 328–339, Mar. 1989.
[29] C. Jörges, C. Berkenbrink, and B. Stumpe, "Prediction and reconstruction of ocean wave heights based on bathymetric data using LSTM neural networks," *Ocean Eng.*, vol. 232, Jul. 2021, Art. no. 109046.
[30] K. Sareen, B. K. Panigrahi, T. Shikhola, and R. Nagdeve, "An integrated decomposition algorithm based bidirectional LSTM neural network approach for predicting ocean wave height and ocean wave energy," *Ocean Eng.*, vol. 281, Aug. 2023, Art. no. 114852.
[31] T. Lin, B. G. Horne, P. Tino, and C. L. Giles, "Learning long-term dependencies in NARX recurrent neural networks," *IEEE Trans. Neural Netw.*, vol. 7, no. 6, pp. 1329–1338, Nov. 1996.
[32] V. Prasad and B. W. Bequette, "Nonlinear system identification and model reduction using artificial neural networks," *Comput. Chem. Eng.*, vol. 27, no. 12, pp. 1741–1754, Dec. 2003.
[33] J. Deng, "Dynamic neural networks with hybrid structures for nonlinear system identification," *Eng. Appl. Artif. Intell.*, vol. 26, no. 1, pp. 281–292, Jan. 2013.
[34] I. B. Tijani, R. Akmeliawati, A. Legowo, and A. Budiyono, "Nonlinear identification of a small scale unmanned helicopter using optimized NARX network with multiobjective differential evolution," *Eng. Appl. Artif. Intell.*, vol. 33, pp. 99–115, Aug. 2014.
[35] V. Sanil Kumar and T. R. Anoop, "Wave energy resource assessment for the Indian shelf seas," *Renew. Energy*, vol. 76, pp. 212–219, Apr. 2015.
[36] O. Nelles, "Nonlinear dynamic system identification," in *Nonlinear System Identification*, 2001, pp. 547–577.
[37] H. Mendonça, "Electricity generation with direct drive wave energy converters: Resistive loading control, grid integration and wave prediction," Ph.D. dissertation, Escuela Técnica Superior de Ingenieros Industriales, Universidad Politécnica de Madrid, Madrid, Spain, 2020.
[38] C. T. Stansberg, "Final report and recommendations to the 23rd ITTC," in *Proc. 23rd Int. Towing Tank Conf.*, 2002, pp. 505–551.
[39] I. R. Young, *Wind Generated Ocean Waves* (Elsevier Ocean Engineering Series), vol. 2. Amsterdam, The Netherlands: Elsevier, 1999.
[40] Government of Canada, Environment Canada. (2014). *National Marine Weather Guide*. [Online]. Available: http://www.ec.gc.ca/
[41] The Coastal Data Information Program. *CDIP Historic Data*. Accessed: Jun. 1, 2025. [Online]. Available: https://cdip.ucsd.edu/
[42] W. S. McCulloch and W. Pitts, "A logical calculus of the ideas immanent in nervous activity," *Bull. Math. Biol.*, vol. 52, nos. 1–2, pp. 115–133, 1990.
[43] S. Haykin, "Neural networks: Principles and practice," *Bookman*, vol. 11, p. 900, Jan. 2001.
[44] M. Sugiyama, H. Sawai, and A. H. Waibel, "Review of TDNN (time delay neural network) architectures for speech recognition," in *Proc. IEEE Int. Symp. Circuits Syst. (ISCAS)*, vol. 1, Mar. 1991, pp. 582–585.
[45] F. Wu, L. P. García-Perera, D. Povey, and S. Khudanpur, "Advances in automatic speech recognition for child speech using factored time delay neural network," in *Proc. INTERSPEECH*, Sep. 2019, pp. 1–5.
[46] Z. Pang, F. Niu, and Z. O'Neill, "Solar radiation prediction using recurrent neural network and artificial neural network: A case study with comparisons," *Renew. Energy*, vol. 156, pp. 279–289, Aug. 2020.
[47] S. Shamshirband, T. Rabczuk, and K.-W. Chau, "A survey of deep learning techniques: Application in wind and solar energy resources," *IEEE Access*, vol. 7, pp. 164650–164666, 2019.
[48] J. Sulaiman and S. H. Wahab, "Heavy rainfall forecasting model using artificial neural network for flood prone area," in *IT Convergence and Security 2017: Volume 1*. Cham, Switzerland: Springer, 2018, pp. 68–76.
[49] L. N. N. Do, H. L. Vu, B. Q. Vo, Z. Liu, and D. Phung, "An effective spatial–temporal attention based neural network for traffic flow prediction," *Transp. Res. C, Emerg. Technol.*, vol. 108, pp. 12–28, Nov. 2019.
[50] T. V. Sushmitha, C. P. Deepika, R. Uppara, and R. N. Sai, "Vehicle trajectory prediction using non-linear input–output time series neural network," in *Proc. Int. Conf. Power Electron. Appl. Technol. Present Energy Scenario (PETPES)*, Aug. 2019, pp. 1–5.
[51] J. Wang, I. Tsapakis, and C. Zhong, "A space–time delay neural network model for travel time prediction," *Eng. Appl. Artif. Intell.*, vol. 52, pp. 145–160, Jun. 2016.

[52] R. Coban, "A context layered locally recurrent neural network for dynamic system identification," *Eng. Appl. Artif. Intell.*, vol. 26, no. 1, pp. 241–250, Jan. 2013.
[53] D. W. Marquardt, "An algorithm for least-squares estimation of nonlinear parameters," *J. Soc. for Ind. Appl. Math.*, vol. 11, no. 2, pp. 431–441, Jun. 1963.
[54] H. Mirzaee, "Long-term prediction of chaotic time series with multi-step prediction horizons by a neural network with Levenberg–Marquardt learning algorithm," *Chaos, Solitons Fractals*, vol. 41, no. 4, pp. 1975–1979, Aug. 2009.
[55] S. Samarasinghe, *Neural Networks for Applied Sciences and Engineering: From Fundamentals to Complex Pattern Recognition*. Boca Raton, FL, USA: CRC Press, 2016.
[56] A. Lloyd, "Seakeeping: Ship behaviour in rough weather," in *Admiralty Research Establishment*. Hoboken, NJ, USA: Wiley, 1989.

H. MENDONÇA (Member, IEEE) was born in Brazil, in 1984. He received the B.Eng. degree in electrical engineering from the Universidade Federal do Maranhão (UFMA), São Luís, Brazil, in 2006, and the M.Sc. degree in electrical engineering and the Ph.D. degree in electrical and electronic engineering from the Universidad Politécnica de Madrid (UPM), Madrid, Spain, in 2012 and 2020, respectively. He is currently an Associate Professor with the Department of Electrical Engineering, Escuela Técnica Superior de Ingenieros Industriales, UPM. His research interests include electrical generation from renewable sources and its integration into the electrical grid, microgrids, ancillary services, and power quality.

S. MARTINEZ (Senior Member, IEEE) was born in Spain, in 1969. He received the M.Sc. degree in industrial engineering and the Ph.D. degree in electrical engineering from the Universidad Politécnica de Madrid, Madrid, Spain, in 1993 and 2001, respectively. He is currently an Associate Professor with the Department of Electrical Engineering, Escuela Técnica Superior de Ingenieros Industriales, Universidad Politécnica de Madrid. His current research interests include electrical generation from renewable energy and the provision of ancillary services from electrical equipment connected to power systems through power electronics.

R. M. DE CASTRO received the Ph.D. degree in industrial engineering from the Universidad Politécnica de Madrid (UPM), Madrid, Spain, in 2013. She is currently an Assistant Professor with the Department of Automatics, Electrical and Electronics Engineering, and Industrial Computing, UPM.